Diffusion Resistances in Alumina and Silica Catalysts

M. RAJA RAO and J. M. SMITH

University of California, Davis, California

Reaction-rate measurements were made for the ortho-para hydrogen conversion at —196°C. at 1 atm. pressure with nickel oxide catalysts using alumina and silica gel as carriers. Data were obtained for fine particles for which pore-diffusion resistances were negligible, for large particles of silica catalyst containing only micropores, and for alumina pellets containing both micro- and macropores. From these data experimental effectiveness factors were evaluated.

Theoretical effectiveness factors predicted by using a previous theory (7) agreed well with the experimental results. The application of the theory requires pore-geometry data. The measurement of these data and their use in predicting diffusion resistances are illustrated by experimental data and calculations for the several catalysts. It is shown that a satisfactory method of predicting the significance of diffusion within porous catalysts requires information on the pore volume and pore sizes.

DIFFUSION RESISTANCES IN ALUMINA AND SILICA CATALYSTS

In catalyst pellets such as those prepared by compressing microporous particles of alumina, the diffusion resistance in the macropores has been found (*3, 6*) to increase rapidly with increasing pellet density. Since the surface area for reaction is predominantly in the microporous particles, the area per unit mass of catalyst does not vary with pellet density. Therefore an optimum density for reaction would exist, in principle, for any pelleted catalyst. It would be desirable to be able to predict this optimum and thus tailor-make catalysts for a given reaction system. For many systems the most desirable density would correspond to effectiveness factors less than unity.

Before such optimization can be attained, it is necessary to be able to relate diffusion rates under reaction conditions to the density of the catalyst pellet. Wakao and Smith have proposed (*6, 7*) a means for accomplishing this that utilizes the effect of density on pore-size distribution and pore volume. These data can now be obtained by comparatively simple laboratory procedures and, together with surface area, constitute required information if both the diffusion and surface reaction resistances are to be identified.

The purpose of this paper is to evaluate the diffusion and reaction theory for high-density alumina pellets where macropore diffusion resistances are large and for a silica gel catalyst carrier which presents the extreme case of zero macropore volume. The other extreme of very low macropore resistance was treated in an earlier paper (*2*). To accomplish this objective the following experimental studies were carried out:

1. Measurement of the rate of reaction under conditions of negligible diffusion resistance. This is necessary in order to determine the rate of the surface processes and was carried out by kinetic studies on fine particles of catalyst.
2. Kinetic measurements for the alumina pellets and large silica gel particles. These results with the data from 1 established experimental effectiveness factors.
3. Determination of pore volumes. pore-size distributions, and particle size distribution for each catalyst in order to predict diffusion rates and, with the data from 1, effectiveness factors.

The ortho-para hydrogen reaction at —196°C. (liquid nitrogen at 1 atm.) and 1 atm. pressure was used for the rate studies. Isothermal conditions within the catalyst were desired in order to limit the overall rate per pellet to a function of diffusion and surface reaction resistances. The low heat of reaction for the hydrogen conversion ensures negligible temperature gradients, even for large pellets. In all cases the catalyst was nickel oxide obtained by decomposing nickel nitrate on the alumina or silica gel carrier. This catalyst was found (*4, 5*) to follow a first-order reaction rate equation at constant pressure and liquid nitrogen temperature.

EXPERIMENTAL

Apparatus

The apparatus used for the kinetic studies is shown in Figure 1. Electrolytic-grade hydrogen was passed through a unit packed with palladium particles to remove oxygen and then through two U-tubes filled with silica gel. The second silica gel tube and the reactor were immersed in a constant temperature bath of liquid nitrogen at atmospheric pressure. A U-tube reactor, ½ in. I.D. and 5 in. in length, constructed of Pyrex glass, was used for experiments with catalyst particles. A tank type of reactor (Figure 1) holding a single pellet was employed for studies with the pellets.

The composition of hydrogen leaving the reactor was measured with a thermal conductivity cell as described by Weitzel and White (*8*). The reference gas was normal hydrogen containing 25% (equilibrium composition at room temperature) of the para form. Both reference and sample streams were passed through the cell, which was operated at a constant current of 165 milliamperes and was maintained at 25°C. with a constant temperature bath. Flow rates through both sides of the cell were measured with soap-film meters. Calibration was effected by operating the reactor with catalyst particles at low flow rates to obtain the equilibrium composition at —196°C. [50.26% para hydrogen (*11*)]. Measurements at successively lower flow rates until the composition showed no further change was assumed to give the equilibrium value. Intermediate compositions were obtained by mixing normal hydrogen and the equilibrium effluent from the reactor.

Catalyst Preparation

A single batch of 7% nickel oxide on aluminum oxide was prepared by soaking boehmite powder in nickel nitrate solution. After impregnation, the material was dried at 110°C. for

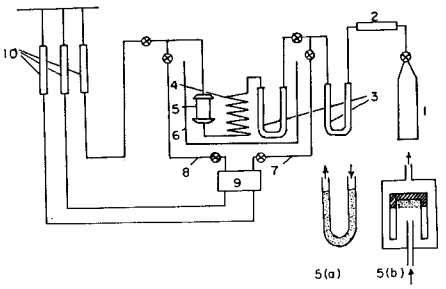

Fig. 1. Schematic flow diagram of apparatus: electrolytic hydrogen cylinder (1), Deoxo unit (2), silica gel tubes (3), precooler (4), flow reactor (5a), single pellet reactor (5b), liquid nitrogen bath (6), reference gas (7), sample gas (8), thermal conductivity cell (9), soap-film meters (10).

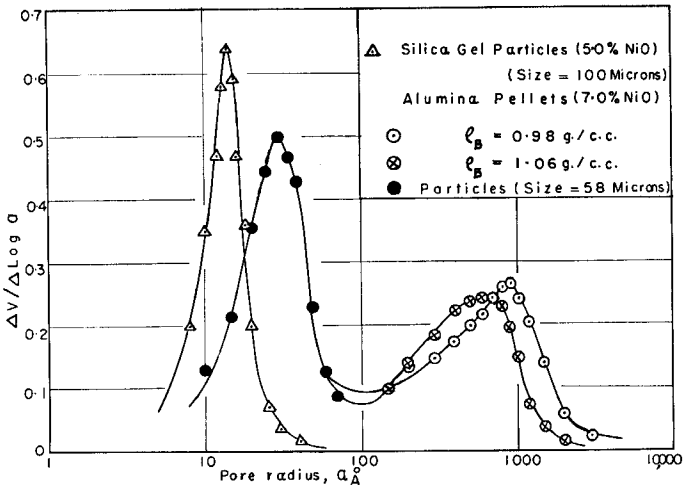

Fig. 2. Pore size distributions of silica and alumina catalysts.

2 hours and then heated at 450°C. for 4 hours. The catalyst was then subjected to a mild grinding operation, and the fraction from 200 to 325 mesh (United States sieve sizes) was used for the kinetic studies. The average particle size, as obtained by the screen analysis, was found to be 58 μ, approximately the same size as that (60 μ) of the original boehmite. The decomposition temperatures of boehmite to aluminum oxide and nickel nitrate to nickel oxide are reported as 360°C. and 400°C., respectively.

A batch of 5% nickel oxide on silica gel was also prepared in a similar manner and two sizes of particles of this catalyst were used for the rate measurements. The average particle diameters of these, evaluated from the screen analysis data, were 1,080 and 100 μ.

Pellets were made from the 7% nickel oxide on aluminum oxide by placing samples of the catalyst particles into a cylindrical mould, 1.0-in. I.D., made of stainless steel. The material was then compressed to a pellet ¼ in. thick. The pellet, still encased in the mould, was inserted in the reactor. Thus only one end face of the cylinder was exposed to the hydrogen mixture, creating a one-dimensional, slab-geometry system for diffusion (see detail sketch in Figure 1). Pellets of two densities 0.98 and 1.06 g./cc. were made and used in the kinetic studies.

For all the rate measurements with particles of catalyst, the particles were supported in the glass reactor on glass wool.

Preliminary runs with an empty reactor and separate experiments with dehydrated aluminum oxide on glass wool showed no activity.

EVALUATION OF RATE CONSTANTS

Catalyst Particles

The rate of hydrogen conversion at constant pressure for the catalyst particles, r_p, can be expressed as

$$r_p = k_W E_i (y_e - y) \tag{1}$$

where y is the mole fraction para hydrogen in the gas stream and E_i is the effectiveness factor for the microporous particle. Gas stream composition can be employed because it has been established (4) that external diffusional resistance is negligible for particles as large as ⅛ in.

The measurements on the particles were carried out in a continuous flow reactor so that

$$r_p\, dW = F\, dy \tag{2}$$

Combining Equations (1) and (2), integrating, and solving for ($k_W E_i$) gives

$$k_W E_i = \frac{1}{W/F} \ln \frac{y_e - y_1}{y_e - y_2} \tag{3}$$

The rate data and values of ($k_W E_i$) calculated from Equation (2) are summarized in Table 1 for the three catalyst particles: 7% nickel oxide on aluminum oxide (mean particle size = 58 μ); 5% nickel oxide on silica

Table 1. Experimental Rate Data
(1 atm., —196°C)

			Flow rate range cc./sec. (25°C., 1 atm.)	W/F range g.(sec.)/(g. mole)	Average value of $k_w E_i \times 10^5$ g. mole/(sec.)(g. cat.)
I.	Catalyst particles	Number of runs			
A.	5.0% NiO on silica gel Mass = 1.0 g. Average particle diameter = 100 μ	7	1.04-2.98	0.082-0.235	4.35
B.	5.0% NiO on silica gel Mass = 1.0 g. Average particle diameter = 1,080 μ	8	1.00-3.18	0.0782-0.249	3.84
C.	7.0% NiO on Al_2O_3 Mass = 1.01 g. Average particle diameter = 58 μ	7	0.985-2.90	0.0883-0.251	4.33
II.	Catalyst pellets				Average value of $(k_w E_i) E_a \times 10^5$ g. mole/(sec.)(g. cat.)
1.	Density, ρ_B = 0.98 g./cc. Mass = 3.14 g.	7	1.09-2.90	0.264-0.702	1.06
2.	Density, ρ_B = 1.06 g./cc. Mass = 3.41 g.	7	1.16-3.51	0.238-0.719	0.870

(1,080 μ); and 5% nickel oxide on silica (100 μ). The total variation in ($k_W E_i$) between runs was about 10% and showed no trend with flow rate.

Catalyst Pellets

The single-pellet reactor was designed to operate (Figure 1) with a constant gas composition on the face of the pellet that corresponded to the exit (y_2) value. Hence the design equation is

$$\bar{r} W = F (y_2 - y_1) \tag{4}$$

where $\bar{r}$ is average reaction rate for the pellet. This rate can be written also in terms of the pellet effectiveness factor E_a as

$$\bar{r} = (k_W E_i) E_a (y_e - y_2) \tag{5}$$

Combining Equations (4) and (5) gives

$$(k_W E_i) E_a = \frac{1}{W/F} \frac{(y_e - y_1)}{(y_e - y_2)} \tag{6}$$

Values of $(k_W E_i)E_a$, evaluated from Equation (6) are given for the two pellets in Table 1.

The ratio of the results for ($k_W E_i$) and $(k_W E_i)E_a$ establish directly an experimental value of E_a for the two alumina pellets. The ratio of ($k_W E_i$) for the silica gel particles establishes the ratio of E_i values for the two sizes of particles.

GEOMETRIC PROPERTIES OF THE CATALYSTS

To evaluate diffusion resistances in the pellets requires mean pore radii and void fractions for the macro and micro regions. To predict E_i for the particles the mean particle size is needed. These properties were determined from experimental measurements as described in the following paragraphs.

Catalyst Powder Particles

The boehmite powder used as a carrier was a spray-dried material. Its properties are given in Table 2. The average particle radius x_p, evaluated from the size-distribution data, is 30 μ. After impregnation with nickel oxide the particles had agglomerated. The material was therefore subjected to a mild grinding operation to break the agglomerations into particles of nearly the same size as the original boehmite. The properties of these catalyst particles were also measured (as described later) and are given in Table 2. The average particle radius of the catalyst particles, computed from the screen analysis, is 29 μ.

The properties of the silica gel carrier (6 to 16 mesh) are listed in Table 2. The properties of the 5% nickel oxide catalyst particles also were measured and are listed in the table. Two sizes of the catalyst were used for the kinetic studies. The coarser grade (10 to 20 mesh) had an average particle radius of 540μ, while the finer fraction had an average radius of 50 μ.

Macropore Characteristics

Macropore void volumes and pore-size distributions were measured for the two alumina catalyst pellets with mercury porosimeter. The right side of Figure 2 shows the pore-size distribution results for the two pellets. Table 3 gives the macropore void fraction ϵ_a determined from the total volume of the pellet and the macropore void volume. Also included in the table are diffusion-average values of the macropore radii. These latter quantities are necessary to evaluate Knudsen diffusion rates in the macropores. The expression for this averaging process, developed in the earlier diffusion paper (6), is

TABLE 2. PROPERTIES OF CATALYSTS AND CARRIERS

Alumina (boehmite)

True density = 2.68 g./cc.

Particle size distribution

μ	% through
90	61.0
60	32.5
45	23.5
20	11.5
10	7.0

Average particle diameter = 60 μ
Surface area = 276 sq. m./g.
Pore volume (N_2) = 0.90 cc./g.
Average pore radius = 23 Å.

7% NiO on Al_2O_3

Particle size distribution

Mesh size Through	On	Weight %
200	250	33.6
250	270	44.0
270	325	22.4

Average particle diameter = 58 μ
True density = 2.63 g./cc.
Surface area = 278 sq. m./g.
Pore volume = 4.40 cc./g.
Average pore radius = 29 Å.
Micropore void fraction in a particle = 0.512

Silica gel (carrier)

Mesh size = 6 to 16
Silica content (dry basis) = 99.6%
True density = 2.20 g./cc.
Average pore radius = 11 Å.
Surface area = 832 sq. m./g.
Pore volume = 0.43 cc./g.

5% NiO on SiO_2

A. Coarser grade

Particle size distribution

Mesh size Through	On	Weight %
10	14	20.2
14	16	40.0
16	20	39.8

Average particle diameter = 1,080 μ

B. Finer grade

Particle size distribution

Mesh size Through	On
120	200

Average particle diameter = 100 μ
True density = 2.31 g./cc.
Pore volume = 0.45 cc./g.
Average pore radius = 12 Å.
Micropore void fraction in a particle = 0.51
Surface area = 630 sq. m./g.

$$\bar{a} = \frac{\int_o^V a\, dV}{V} \tag{7}$$

From the pellet density, ρ_B, and ϵ_a, the density ρ_p of the microporous particles can be determined. The particle densities for the two pellets were almost the same, indicating that the particles were not crushed in the pelleting process. An average value of the particle density was used to evaluate the micropore void fraction given in the following section.

Micropore Characteristics

A sorptometer using the nitrogen-helium system was employed to measure the complete adsorption equilibrium curves for the silica (average particle diam. 100 μ) and alumina catalyst particles. In this device an equilibrium quantity of nitrogen is first adsorbed on the catalyst at liquid nitrogen temperature. Then the bed is warmed to room temperature and the amount desorbed is measured. Successive desorption measurements of this type determined the equilibrium adsorption curves shown in Figure 3. From these measurements the micropore volumes and pore-size distribution curves were obtained. The latter results are shown on the left side of Figure 2. By connecting the micro and macro sections of the curves for the

TABLE 3. PORE GEOMETRY PROPERTIES OF CATALYST PELLETS (7% NiO on Al_2O_3)

Pellet diameter = 1 in.; thickness = ¼ in.; volume = 3.22 cc.

W grams	Pellet density ρ_B-g./cc.	Particle density ρ_p g./cc.	Macropores* Void fraction ϵ_a	Macropores* Average pore radius $\bar{a}_a$, Å.	Micropores† Void fraction ϵ_i	Micropores† Average pore radius $\bar{a}_i$, Å.
3.14	0.98	1.23	0.20	920	0.39	29
3.41	1.06	1.32	0.192	652	0.42	29

* ϵ_a, $\bar{a}_a$ values are evaluated from the pore-size distribution data, measured with mercury porosimeter.

† ϵ_i, $\bar{a}_i$ values are obtained from the micropore size distribution of the powder particles, measured with sorptometer.

alumina catalysts, a complete pore-size distribution is obtained for these two pellets.

The surface areas were obtained from the adsorption curves (Figure 3) by the standard B-E-T method and were listed together with the measured pore volumes in Table 2 for the two catalysts. It is noted that the nickel oxide on silica catalyst has a relatively higher surface area with a narrow size range of fine pores. The average radius of these micropores, evaluated from the pore-size distribution data with the help of Equation (7) was 12 Å. On the other hand, the nickel oxide and aluminum oxide have a comparatively lower surface area and a broader spectrum of the sizes of the micropores, giving an average pore radius of 29 Å.

From the measured pore volume and the true density, the micropore void fraction ϵ_{ip} was evaluated for the silica catalyst. The true density for this catalyst was estimated from the density of silica gel (Table 2) by accounting for the mass change in adding nickel oxide; thus ρ_t = 2.20 (105/100) = 2.31 g/c.c. For the pellets of nickel oxide on aluminum oxide, the micropore void fractions, ϵ_i were computed from the average particle density and the measured micropore volume. These results are given in Tables 2 and 3.

THEORETICAL AND EXPERIMENTAL EFFECTIVENESS FACTORS

Microporous Particles (E_i)

When only micropores exist, as in particles of the aluminum oxide or silica gel catalyst, it has been shown (7) that the effectiveness factor E_i is given by the equations

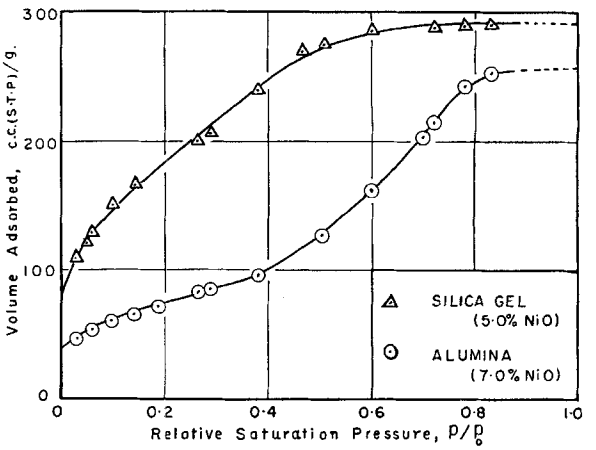

Fig. 3. Adsorption isotherms (nitrogen at −196°C.) for silica and alumina catalysts.

$$E_i = 3\frac{h_i \coth h_i - 1}{h_i^2} \tag{8}$$

$$h_i = x_p \sqrt{\frac{k_w \rho_p RT}{D_{ip} P}} \tag{9}$$

$$D_{ip} = \frac{\epsilon_{ip}^2}{(1-\alpha y)/D_b + 1/\overline{D}_{ki}} \tag{10}$$

These results are based upon the Wheeler (*10*) approach, but extend it by proposing a means of predicting the diffusivity of a microporous particle in terms of bulk (D_b) and Knudsen diffusivities ($\overline{D}_{ki}$), and the pore void fraction ϵ_{ip}. The equations are based upon the assumption of a first-order reaction and spherical particles. For the equal-molal counter diffusion encountered in the ortho-para hydrogen reaction, $\alpha = 0$ so that Equation (10) becomes

$$D_{ip} = \frac{\epsilon_{ip}^2}{1/D_b + 1/\overline{D}_{ki}} \tag{11}$$

At −196°C., the bulk diffusivity of hydrogen from the data of Jost (*1*) is 0.14 sq. cm./sec. The micro-Knudsen diffusivity $\overline{D}_{ki}$ is evaluated from the expression

$$D_k = 2/3\,\bar{a}\,\bar{v} \tag{12}$$

Substituting these results in Equation (11) gives a value of D_{ip} for each catalyst. Equations (8) and (9) provide a relationship between k_w and E_i. The product ($k_w E_i$) is available from the rate measurements on particles (Table 1) so that E_i can be evaluated by trial. The results given in Table 4A show that h_i is so low for both the aluminum

TABLE 4. EXPERIMENTAL AND THEORETICAL EFFECTIVENESS FACTORS

A. Catalyst particles

Catalyst	Average particle radius (μ)	D_{ip} sq. cm./sec.	h_i	E_i Predicted	E_i Measured
7% NiO on Al_2O_3	29	0.00407	0.027	1.0	
5% NiO on SiO_2	50	0.00179	0.066	1.0	
5% NiO on SiO_2	540	0.00179	0.69	0.95	0.89

B. Catalyst pellets

Catalyst	Pellet density g./cc.	Diffusivity, D, sq. cm./sec. Macro contribution	Micro-series contribution	Total	h_L	E_a Predicted	E_a Measured
7% NiO on Al_2O_3	0.98	0.00446	0.00477	0.00923	3.42	0.28	0.25
7% NiO on Al_2O_3	1.06	0.00380	0.00541	0.00921	3.57	0.27	0.20

oxide catalyst particles and the small size (50 μ radius) silica gel catalyst that E_i is unity. However, for the larger particles of silica gel catalyst (x_p = 540 μ) a value of E_i = 0.95 is predicted.

Since E_i = 1.0 for the small silica catalyst particles, the product ($k_W E_i$) in Table 1A gives the value of the rate constant k_W. With this rate constant and the ($k_W E_i$) product for the larger particles, Table 1B, an experimental value of E_i = 0.89 is obtained in comparison with the predicted result of 0.95.

It appears that E_i will be close to unity except for very rapid reactions and exceptionally large particles. The silica gel case emphasizes the importance of diffusion resistance because of the small pore radii, and even here E_i is of the order of 0.9 for 1,080 μ particles.

Pellets (E_a)

The solution for E_a for slab, cylinder, or spherical pellets for a first-order reaction was presented in reference 7. For the ortho-para hydrogen reaction (α = 0) and one-dimensional diffusion (slab geometry) from one face only, an analytical solution is possible according to the equations

$$E_a = \frac{\tanh h_L}{h_L} \tag{13}$$

$$h_L = L\sqrt{\frac{(k_W E_i)\,\rho_B\,RT}{DP}} \tag{14}$$

$$D = \frac{\epsilon_a^2}{\dfrac{1}{D_b} + \dfrac{1}{\overline{D}_{ka}}} + \frac{\epsilon_i^2(1 + 3\epsilon_a)}{(1 - \epsilon_a)} \frac{E_i}{\dfrac{1}{D_b} + \dfrac{1}{\overline{D}_{ki}}} \tag{15}$$

This diffusivity expression is based upon a model which takes into account three parallel contributions: diffusion through the macropores, micropores, and a series contribution involving both types of pores. In Equation (15) the first term represents the macropore contribution and the second the sum of the micro and series contributions.

These equations can be applied to the alumina catalyst pellets by first evaluating the diffusivity D. This is done using Equation (15) and the pellet properties given in Table 3. The macro-Knudsen diffusivity was evaluated from Equation (12). The results, given in Table 4B, show the separate contributions to the diffusivity as well as the total. Knowing D, and ($k_W E_i$) from the rate measurements on the aluminum oxide catalyst particles, Equations (13) and (14) determine the pellet effectiveness factor. The resultant values of E_a are given in the next to the last column of Table 4B for the two pellets. For comparison, measured effectiveness factors can be obtained from the ($k_W E_i$)E_a and ($k_W E_i$) data given in Table 1 for the pellets and particles of the aluminum oxide catalyst.

DISCUSSION

The silica and alumina catalysts studied in this investigation and the data for the alumina pellets reported earlier (2) cover a wide range of diffusion resistances, and, hence, effectiveness factors. The theory for the effect of pore geometry on effectiveness factors predicts results which agree reasonably well with experimental data over the entire range. At the one extreme (silica gel catalysts) where only micropores are involved the effectiveness factors are high despite the small pore radii. This is because the particles themselves are small. At the other extreme, large pellets and small macropores, the effectiveness factors are small. This situation is illustrated for the 7.0% nickel oxide on aluminum oxide pellets reported in this work. Because of the small macropores, the macro contribution to the diffusivity shown in Table 4B was less than half of the total, and the effectiveness factor was but 0.2 to 0.3. The earlier work utilized the same reaction and conditions, but the more active (25% nickel oxide) catalyst pellets had larger macropore radii ($\overline{a_a}$ 1,200 to 2,100 Å vs. 652 to 920 Å). Here the diffusion resistances were comparatively different, the macro contribution being 90% of the total diffusivity. Predicted and experimental effectiveness factors agreed well in this case also, and ranged from 0.16 to 0.30 for three pellets of different densities.

The application of the theory to alumina and silica porous carriers may not be satisfactory for all other reactions and porous catalysts. For example in cases where surface diffusion is significant, the theory would not be applicable. Also diffusion rates are based (6) upon a random distribution of pores with numerous interconnections. Hence, materials which are more like an assembly of capillary tubes would not be treated satisfactorily by the theory.

ACKNOWLEDGMENT

The financial support for this work was provided by the United States Army Research Office (Durham), Grant No. DA-ARO(D)-31-124-G191.

NOTATION

$\overline{a_a}$ = average macropore radius, cm.
$\overline{a_i}$ = average micropore radius, cm.
D = effective diffusivity of hydrogen in catalyst pellet, sq. cm./sec.
D_{ip} = effective diffusivity of hydrogen in catalyst particle, sq. cm./sec.
$\overline{D}_{ka}$ = average macro-Knudsen diffusivity in the macropores, sq. cm./sec.
$\overline{D}_{ki}$ = average micro-Knudsen diffusivity in the micropores, sq. cm./sec.
D_b = bulk (molecular) diffusivity of hydrogen, sq. cm./sec.
E_i = effectiveness factor (micropore) for catalyst particles
E_a = effectiveness factor (macropore) for catalyst pellet
F = flow rate, g. moles/sec.
k_W = specific reaction rate, (g. mole)/(sec.) (g. cat.)
L = thickness of the catalyst pellet, cm.
h_i = Thiele parameter for spherical particles
h_L = Thiele parameter for a catalyst pellet of slab geometry
p = partial pressure of nitrogen, atm.
P = total pressure, 1 atm.
p_o = saturation pressure of liquid nitrogen at −196°C., 1 atm.
r_p = rate of production of para hydrogen, (g. moles)/(sec.) (g. cat.) for the catalyst particles
$\overline{r}$ = average rate of reaction for the catalyst pellet (g. moles)/(sec.) (g. cat.)
R = gas constant, (cc.) (atm.)/(g. mole) (°K.)
T = temperature, °K.
$\overline{v}$ = mean molecular velocity of hydrogen (at −196°C), cm./sec.
V = pore volume, cc./g.
W = weight of the catalyst, g.
x_p = mean radius of the catalyst powder particles, cm.
y = mole fraction of para hydrogen in the gas stream or in macropores
y_e = equilibrium value of para hydrogen concentration at −196°C., 0.5026

Greek Letters

α = (1 + ratio of diffusion rates of two components); α = 0 for equal-molal counter diffusion

ρ_B = pellet density, g./cc.
ρ_p = particle density, g./cc.
ρ_t = solid density, gm./cc.
ϵ_a = macropore void fraction in a pellet
ϵ_i = micropore void fraction in a pellet
ϵ_{ip} = micropore void fraction in particle

Subscripts

1 = entrance of the reactor
2 = exit of the reactor

LITERATURE CITED

1. Jost, W., "Diffusion," Verlag Von Steinkopff, Darmstadt, Germany (1957).
2. Rao, M. Raja, N. Wakao, and J. M. Smith, "Diffusion and Reaction Rates for Ortho-hydrogen Conversion," submitted to *Ind. Eng. Chem.*
3. Robertson, J. L., and J. M. Smith, *A.I.Ch.E. Journal*, **9**, No. 3, p. 342 (1963).
4. Wakao, N., P. W. Selwood, and J. M. Smith, *A.I.Ch.E. Journal*, **8**, 478 (1962).
5. ————, J. M. Smith, and P. W. Selwood, *J. Catalysis*, **1**, 62 (1962).
6. Wakao, N., and J. M. Smith, "Diffusion in Catalyst Pellets," *Chem. Eng. Sci.*, **17**, 825 (1962).
7. ————, "Diffusion and Reaction Rates for Porous Catalysts," submitted to *Ind. Eng. Chem.*
8. Weitzel, D. H., and L. E. White, *Rev. Sci. Instr.*, **26**, 290 (1955).
9. Wheeler, Ahlborn, "Advances in Catalysis," Vol. 3, p. 250, Academic Press, New York (1950).
10. ————, "Catalysis," Vol. 2, p. 105, Reinhold, New York (1955).
11. Woolley, H. W., R. B. Scott, and F. G. Brickwedde, *J. Res. Nat'l Bur. Std.*, **41**, 379 (1948).

Manuscript received November 26, 1962; revision received April 1, 1963; paper accepted April 2, 1963.

A High Resolution Resistivity Probe for Determination of Local Void Properties in Gas-Liquid Flow

L. G. NEAL and S. G. BANKOFF

Northwestern University, Evanston, Illinois

Although considerable research has been devoted to the study of concurrent flow of gas—liquid or vapor—liquid mixtures, many details of the basic flow structure remain unknown. An important reason has been the lack of instrumentation capable of precise measurement of local parameters, such as local volumetric gas fraction, bubble frequency, and local bubble size distribution.

Most previous studies have used techniques which measured gas fractions averaged over the channel cross section. These methods employ the attenuation of gamma rays and beta rays (*1, 2, 3*); radioactive tracers (*4*); photographic records (*5*); and weighing a test section (*6*) The most popular of these is the gamma-ray technique, in which gamma rays from a radioactive source are passed through the stream. The strength of the attenuated beam is a function of the stream density and hence related to the gas fraction.

Hooker and Popper (*1*) have studied this method at some length and include an uncertainty analysis in their report. They concluded, from work with lucite mock-ups corresponding to gas concentrated at particular locations within the channel, that the gamma-ray technique was unsatisfactory for nonhomogeneous flow. Cook (*8*) and Egen (*7*) reported errors as large as 93% in annular flow. This source of error is common to all techniques which measure cross-sectional average gas fractions.

The gamma technique was improved by Petrick (*2*) who used a traversing method in which the source and detector were moved across the channel to get a gas fraction profile. The cross-sectional average gas fraction was obtained by integration of this profile. The advantage of the traversing technique is that an average is made over only one space coordinate; this reduces errors due to nonuniform gas distribution. Further, it gives a rough approximation to the gas fraction profile. The gamma-ray method is reasonably accurate for determining cross-section average gas fractions when the gas is uniformly distributed; the test section offers a radiation path greater than 1 in. of water, and the gas fraction is greater than 0.25. However, the method detects space-average rather than local values of the gas fraction and gives no information on individual bubble frequencies and size distributions. Recently radial void fractions have been obtained by the traversing technique with a polynomial-fitting procedure (*14*).

Several cases are reported in the literature of the use of probing techniques to measure local parameters in two-phase flow. Krasiakova (*9*) used a hot-wire anemometer to measure liquid film thickness in horizontal annular flow. McManus (*10*) used a precalibrated capacitance probe to measure the thickness of the liquid film for the same case. Hewitt (*11*) used a capacitance probe to measure film thickness in vertical flow. Both techniques were used to measure surface wave frequency and height. Solomon (*12*) has employed a conductivity probe as a flow regime indicator in air-water flow.

In this work an electrical resistivity probe is described which is capable of measuring local values of the volumetric gas fraction, bubble frequencies, and local bubble size spectra in a mercury-nitrogen system, where the output appears as a random square wave. Analysis of this signal in terms of autocorrelation functions and power density spectra is expected to provide valuable new information concerning the structure of two-phase flow.

DEFINITION OF TERMS

Before discussing the instrument, the variables to be measured should be clearly defined. Bubble frequency and bubble size distribution at a point are, respectively, the number of bubbles that pass through the point per unit

L. G. Neal is with the Norwegian Institute for Atomic Energy, Kjeller, Norway.